DE GRUYTER Z. Phys. Chem. 2017; 231(7–8): 1423–1442

Johanna Uhlendorf, Benjamin Ruprecht, Elena Witt, C. Vinod Chandran, Lars Dörrer, Erwin Hüger, Florian Strauß, Paul Heitjans and Harald Schmidt*

# Slow Lithium Transport in Metal Oxides on the Nanoscale

DOI 10.1515/zpch-2016-0939
Received November 22, 2016; accepted June 1, 2017

**Abstract:** This article reports on Li self-diffusion in lithium containing metal oxide compounds. Case studies on $LiNbO_3$, $Li_3NbO_4$, $LiTaO_3$, $LiAlO_2$, and $LiGaO_2$ are presented. The focus is on slow diffusion processes on the nanometer scale investigated by macroscopic tracer methods (secondary ion mass spectrometry, neutron reflectometry) and microscopic methods (nuclear magnetic resonance spectroscopy, conductivity spectroscopy) in comparison. Special focus is on the influence of structural disorder on diffusion.

**Keywords:** ionic conductivity; lithium self-diffusion; metal oxides; neutron reflectometry; NMR spectroscopy; secondary ion mass spectrometry.

## 1 Introduction

For the investigation of Li self-diffusion in Li containing solids basically microscopic methods [e.g. nuclear magnetic resonance (NMR) spectroscopy] and

***Corresponding author: Harald Schmidt,** Technische Universität Clausthal, Institut für Metallurgie, AG Mikrokinetik, Clausthal-Zellerfeld, Germany; ZFM – Zentrum für Festkörperchemie und Neue Materialien, Hannover, Germany; and CZM – Clausthaler Zentrum für Materialtechnik, Clausthal-Zellerfeld, Germany, e-mail: harald.schmidt@tu-clausthal.de
**Johanna Uhlendorf, Lars Dörrer and Erwin Hüger:** Technische Universität Clausthal, Institut für Metallurgie, AG Mikrokinetik, Clausthal-Zellerfeld, Germany
**Benjamin Ruprecht, Elena Witt and C. Vinod Chandran:** Institut für Physikalische Chemie und Elektrochemie, Leibniz Universität Hannover, Hannover, Germany
**Florian Strauß:** Technische Universität Clausthal, Institut für Metallurgie, AG Mikrokinetik, Clausthal-Zellerfeld, Germany; Institut für Physikalische Chemie und Elektrochemie, Leibniz Universität Hannover, Hannover, Germany; and CZM – Clausthaler Zentrum für Materialtechnik, Clausthal-Zellerfeld, Germany
**Paul Heitjans:** Institut für Physikalische Chemie und Elektrochemie, Leibniz Universität Hannover, Hannover, Germany; and ZFM – Zentrum für Festkörperchemie und Neue Materialien, Hannover, Germany

macroscopic tracer methods (e.g. secondary ion mass spectrometry, not, however, the common radiotracer technique) can be used. Microscopic methods allow the determination of correlation times or jump rates, often for diffusion lengths in the order of some atomic distances, i.e. on the nanoscale. The diffusivity, $D$, can be calculated indirectly using model assumptions. In contrast, with macroscopic tracer methods it is possible to detect long-range diffusion processes with a large number of jumps. Diffusivities can be determined directly by measuring the diffusion length, $d = (6Dt)^{1/2}$, ($t$: time) which is the average displacement of atoms during the diffusion event. The comparison of both types of methods on the same material will give synergetic information and a comprehensive picture on diffusion properties, especially if they are applied on the overlapping time and length scales of the diffusion process.

Fast Li diffusion processes in solids, generally taking place in ion-conductors, are routinely studied in literature due to their importance for battery materials. In contrast, slow diffusion processes are investigated less often (references see below). Nevertheless, they are likewise of fundamental interest in order to obtain a coherent general view. A classic example is the occurrence of slow collective migration of several atoms in disordered solids. Differences in diffusion behavior on long time scales in comparison to short time scales will indicate important changes of the diffusion mechanism. In addition, the study of slow diffusion processes is important for understanding materials' stability. Self-diffusivities determine the intrinsic stability of metastable materials like glasses or nanocrystalline materials (crystallization, grain growth, structural relaxation). In this context, diffusion on short length scales of some nanometers is of special interest due to the given structural peculiarities. In the present paper, the study of the influence of structural disorder on diffusion was also attributed to the question: how differs diffusion in solids with the same chemical composition but with a different structural state/type of order? Comparative experiments on amorphous, nano-crystalline and single crystalline samples will elucidate how diffusion can be accelerated or slowed down by structural modifications in view of applications in solid electrolytes and materials stability.

For the determination of slow diffusivities in solids by macroscopic tracer methods, secondary ion mass spectrometry (SIMS) and neutron reflectometry (NR) are well suited and applied in this study. In combination, diffusivities between $10^{-15}$ and $10^{-25}$ $m^2/s$ at diffusion lengths of 0.5 nm to several mm can be determined [1]. A method which can reveal diffusion processes on the microscopic length scale and which can also very well be used to study slow diffusion processes is spin-alignment echo-NMR (SAE-NMR) [2–4]. Here, diffusivities down to $10^{-20}$ $m^2/s$ at diffusion lengths of 1 nm can be detected [5–7]. In addition, impedance/conductivity spectroscopy which depending on the measuring frequency

yields information on the long-range ion transport or local ion hopping [8], was applied for comparison. As model systems lithium metal oxides like $LiNbO_3$, $Li_3NbO_4$, $LiTaO_3$, $LiAlO_2$, and $LiGaO_2$ were investigated as case studies.

Investigations on self-diffusion in Li containing solids were done in recent years nearly exclusively by NMR methods including beta-NMR and muon-spin spectroscopies [2, 9–15] which allow a characterization of fast as well as slow, generally short-range diffusion processes. In addition, conductivity measurements were done for an indirect characterization of diffusion [13, 16]. Tracer experiments are nearly completely lacking. This is due to the fact that suitable radioactive tracers are not available and the natural abundance of the stable Li isotopes is high (see below). Consequently, in literature only some special publications can be found. There are experiments based on the radio tracer method using the prompt alpha-decay following the beta-decay of the short-lived isotope $^8$Li ($t_{1/2} = 0.84$ s) [17]. Such elegant experiments are, however, of low significance for slow diffusivities due to the limited annealing time period available. Investigations with the stable $^6$Li tracer were done with SIMS [18–21]. In this context, also chemical diffusivities were measured [18].

The experimental investigation of Li diffusion in inorganic materials by NR is a relatively new topic. Literature work is mainly on the investigation of self-diffusion in thin metallic, semiconducting and ceramic films in form of isotope multilayers [1, 22–26]. One of the main achievements of the present work was to implement an improvement of the classical multilayer technique [27, 28], where self-diffusion in bulk materials was measured by NR for the first time and to transfer the method to the application to lithium.

The present article reviews already published research of the authors on the topic discussed above and gives additional new results. The latter are clearly indicated throughout the paper.

# 2 Experimental

## 2.1 Tracer methods

In general, self-diffusion experiments using Li tracers are connected with a variety of analytical problems. First of all, for lithium no suitable (long-lived) radioactive tracers are available for the performance of extensive diffusion measurements. This prevents the use of the standard radiotracer technique, which is state-of-the-art in diffusivity determination in metals or intermetallics due to its high detection sensitivity [29]. To circumvent this problem, it is necessary to use

rare stable isotopes. Lithium has two stable isotopes: $^{6}$Li with a natural abundance of 7.5 % and $^{7}$Li with an abundance of 92.5 %, where $^{6}$Li can be used as a 'rare' stable tracer.

In general, a classical tracer experiment is done in the following way: (i) Deposition of the $^{6}$Li tracer on top of or into the sample under investigation, (ii) diffusion annealing for the thermally activated motion of Li ions into the solid, (iii) analysis of the initial and modified time and space dependent $^{6}$Li concentration by appropriate analytical tools (creation of isotope depth profiles), and finally (iv) least-squares fitting of the $^{6}$Li profiles with appropriate solutions of the diffusion equation using adequate boundary conditions.

For lithium self-diffusion experiments in lithium containing solids with stable isotopes problems arise due to the relatively high natural abundance of $^{6}$Li isotopes of 7.5 %. This considerably decreases the detection sensitivity of the tracer within a solid with natural isotope composition under investigation and it is hard to detect concentration changes of $^{6}$Li by diffusion, due to the relatively high natural abundance. Consequently, for classical tracer deposition methods like ion implantation or the deposition of a thin lithium layer on top of the surface, the natural isotope background of the sample under investigation is often too high. The Li tracer in low concentrations is simply not detectable. On the other hand, the use of higher amounts of tracer leads to chemical inhomogeneities, which will result in unwanted chemical diffusion. Another possibility, tracer deposition by ion-implantation in high doses has also the consequence of a strong distortion of the structural state and of the point defect equilibrium of the sample up to unwanted amorphisation. Tracer deposition from a $^{6}$Li enriched gas phase via $^{6}$Li/$^{7}$Li gas-exchange might be limited by surface exchange processes (transfer of atoms across the gas/solid interface).

A well suited technique of tracer deposition in lithium containing solids is the use of isotope heterostructures [30–33]. There, on top of a bulk crystal or a thin film of a material with natural isotope composition under investigation $Li_xA$ (A: arbitrary species or combination of species; $x$: relative lithium fraction), a material of identical or almost identical chemical composition is deposited, which, however, is enriched with $^{6}$Li. This gives a structure of $^{6}Li_xA/Li_xA$. For the deposition of several nanometer thin $^{6}Li_xA$ layers ion beam sputtering is used as described in [34]. The sensitivity of the method is enhanced if the sample to be investigated is also isotope enriched, but with $^{7}$Li. Then, $^{6}Li_xA/^{7}Li_xA$ structures are formed.

During diffusion annealing, interdiffusion of the two stable Li isotopes takes place without a modification of the homogeneous chemical composition of the structure. Consequently, pure tracer self-diffusion is measured. For long annealing times, the $^{6}$Li tracer penetrates deeply into the material under investigation.

For a derivation of the diffusivity, the $^6$Li concentration or atomic fraction is determined as a function of depth by SIMS or NR.

### 2.1.1 Secondary ion mass spectrometry (SIMS)

After tracer deposition first the $^6$Li isotope mole fraction of the as-deposited sample, $c_0(x)$, is measured by SIMS as a reference. After annealing the initial mole fraction is modified to $c(x,t)$, where $x$ is the space coordinate and $t$ the annealing time. Classical $^6$Li isotope mole fractions as obtained by SIMS analysis during annealing are shown in Figure 1a for the case of $LiNbO_3$. The penetration of the tracer into the sample with increasing annealing time due to diffusion is clearly visible. The depth profiles are fitted by solutions of Ficks second law, choosing adequate starting and boundary conditions [35], depending on the spatial extension of the tracer layer as given by $c_0(x)$. Typical examples are the thin film solution and the thick film solution [see Equation (1)]. A parameter, $R$, describing the "broadening" of the initial profile, $R_0$, during annealing is extracted by a least-squares fitting procedure. This allows one to determine the diffusivity due to $D=(R^2-R_0^2)/4t$. In case of the example given in Figure 1b, the solution is

$$c(x,t)=c_\infty+\frac{(c_0-c_\infty)}{2}\left[\mathrm{erf}\left(\frac{h+x}{R}\right)+\mathrm{erf}\left(\frac{h-x}{R}\right)\right] \tag{1}$$

where $c_\infty$ is the natural abundance of $^6$Li in the sample and $h$ the original thickness of the as-deposited tracer layer. SIMS investigations were carried out using

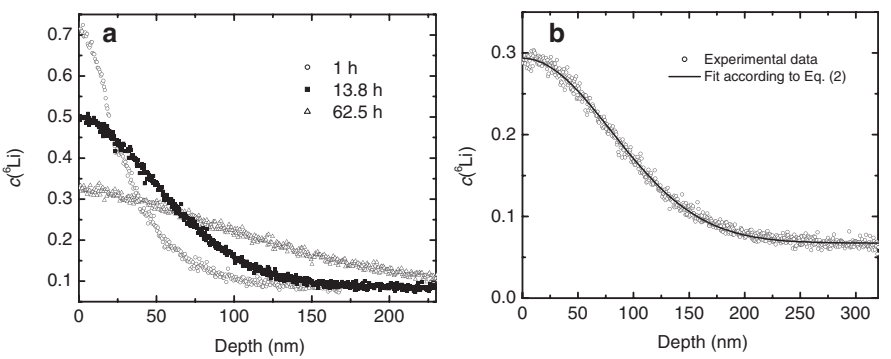


**Fig. 1:** (a) Atomic fraction of $^6$Li as a function of depth for a $^6LiNbO_3$ (30 nm)/$LiNbO_3$ (single crystal) structure annealed at 523 K or 1, 13.8 and 62.5 h. (b) Atomic fraction of $^6$Li as a function of depth after annealing at 473 K for 34 days. A least-squares fit of Equation (1) to the experimental data is also indicated [34] – reproduced by permission of the PCCP Owner Societies.

a "Cameca ims 3f/4f" machine. Due to electrical charging during the measurements, we used an $O^-$ primary ion beam (15 keV, 50 nA). The sputtering area was of $250 \times 250\ \mu m^2$. For analysis of the isotopes in a double-focused mass spectrometer, the signal resulting from an area of about $60 \times 60\ \mu m^2$ in the center of the sputtering area was used to exclude crater-edge effects.

The secondary ion intensities of the two lithium isotopes, $I(^6Li^+)$ and $I(^7Li^+)$, were recorded as a function of sputter time in depth-profiling mode. Since the two lithium isotopes are chemically identical (neglecting the small isotope effect), for diffusion analysis, the intensity of the signals was converted into $^6Li$ atomic fractions $c$ according to

$$c = \frac{I(^6\mathrm{Li})}{I(^6\mathrm{Li}) + I(^7\mathrm{Li})} \tag{2}$$

Depth calibration of each sputter crater was realized by measuring the depth with a mechanical profilometer (Tencor, Alphastep).

### 2.1.2 Neutron reflectometry (NR)

For diffusion studies by NR the sample was composed of a commercial single crystal where a 50 nm thick amorphous $^6LiNbO_3$ layer was sputter deposited on top. During NR measurements (specular mode) a beam of neutrons is directed on the sample surface at small incident angles, which is reflected at interfaces between layers with different neutron scattering length densities. These are the isotope interface between $^6LiNbO_3/LiNbO_3$ and the surface. Due to interference effects, typical reflectivity patterns are measured, as shown in Figure 2a, where the reflectivity $R$ (the number of incoming neutrons divided by the number of reflected neutron) is plotted as a function of the scattering vector $q_z = 4\pi/\lambda \sin(\theta)$. Figure 2a gives an example for a sample in the as-deposited state and after diffusion annealing in comparison. The differences in the two patterns are clearly visible. In order to derive diffusivities, the reflectivity patterns were computer modeled and least-squares fitted by the parratt32 [36] software tool [28]. This results in a scattering length density (SLD) profile based on a layer model as shown in Figure 2b. The SLD of the annealed sample which is dependent on the mole faction of $^6Li$ clearly indicates diffusion into the bulk sample. Due to the fact that no chemical gradients are present, the tracer diffusion of Li into the single crystal is monitored. Diffusivities are again extracted by comparing initial and diffused state. Due to the complexity of the analysis and for a deepened understanding it is referred to Ref. [28] for further reading. The NR method described

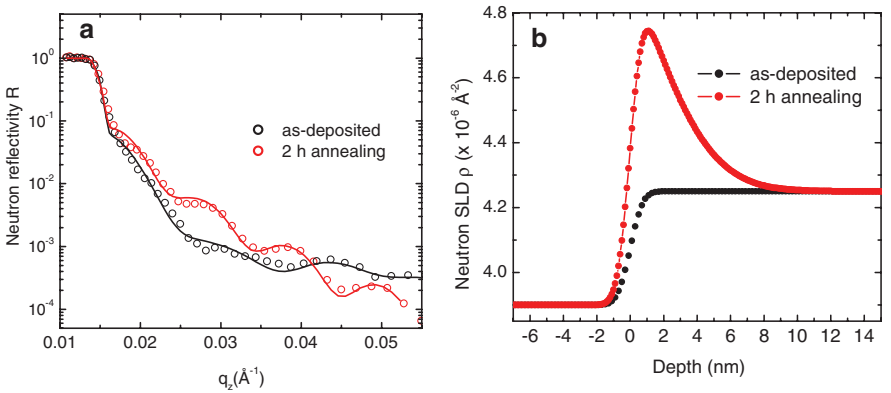


**Fig. 2:** (a) Measured NR patterns (open symbols) and corresponding Parratt32 simulations (lines) for a $LiNbO_3$ single crystal with a deposited $^6LiNbO_3$ film on top in the as-deposited state and after annealing at 473 K for 2 h. (b) SLD as obtained from the Parratt32 simulations in (a). The space coordinate is set to zero at the film/crystal interface. The diffusion length of the annealed sample is 2.5 nm (for details see also [28]).

allows to determine diffusion lengths in the range between 1 and 10 nm, i.e. diffusion on the nanoscale, similar to microscopic methods such as NMR.

## 2.2 Ionic conductivity measurements

When measuring the ionic conductivity $\sigma$ of a material with a direct current (dc) applied a reservoir of the conducting ionic species is needed as an electrode on both sides. In case of the slow Li conductors discussed here this ideal setup is in conflict with other boundary conditions, e.g. the need for high temperatures above the melting point of elementary Li and an oxidizing atmosphere preventing additional oxygen deficiency in the material. On the other hand, by using non-Li electrodes the ions are blocked at the interface to the sample material. This effect can be mitigated by regularly changing the polarity, i.e. an alternating current (ac) measurement setup, which effectively leads to probing the material over a wide frequency range.

The impedance measurements were carried out using polished samples contacted with ion blocking Ag electrodes which were kept in an oxidizing atmosphere, i.e. air, while they were heated in the cell. For the typical frequency range from 10 mHz to 1 MHz the regime of the characteristic so-called dc plateau and the dispersive regime could be recorded, as well as the reduction of the conductivity at low frequencies due to the ionic blocking effects mentioned. The dc plateau

represents the long-range conductivity of the material as neither the ionic blocking effect nor dispersive behavior significantly contribute to its value.

Since low-conductivity materials were probed, the samples were only heated, but not cooled in order to adjust their conductivities to the sensitivity range of the impedance analysers (<$10^{-7}$ S), leading to a temperature range between room temperature and up to about 950 K. Thus, roughly eight orders of magnitude in the conductivity could be covered by the measurements [37].

## 2.3 $^{7}$Li NMR spectroscopy

NMR spectroscopy allows contactless probing of the Li motion in the sample material. Depending on the temperature and therefore the ionic hopping rate several NMR techniques sensitive to different time windows of the Li motion can be used. Here, $^{7}$Li spin-lattice relaxation NMR (SLR-NMR), $^{7}$Li spin-alignment echo NMR (SAE-NMR) and motional narrowing analysis of solid state $^{7}$Li NMR spectra were applied [38].

In SLR-NMR transients of the relaxation of the perturbed longitudinal magnetization of the probe nuclei ensemble are recorded. The temperature dependence of the relaxation rates $T_1^{-1}$ shown by the transients gives access not only to the activation energy of the short-range and the long-range ionic motion, respectively, but also to the absolute correlation rates $\tau^{-1}$ of the motion, which can be identified as the ionic hopping rate. In SLR-NMR different models exist for the shape of the characteristic $T_1^{-1}$ rate peak that also take into account the dimensionality of the motion [12, 39, 40]. As the peak appears around the temperature where the correlation rate is similar to the Larmor precession frequency induced by the external magnetic field, SLR-NMR is mainly applicable at high temperatures.

A more direct, i.e. model independent NMR technique is SAE-NMR [5, 7]. It is based on the idea of a solid-echo pulse sequence where the second 90° pulse is "split" into two 45° pulses by a mixing time $t_m$. This sequence is known as the Jeener–Broekaert-pulse sequence [41]. It has been shown that the decay rate of the echo amplitude with $t_m$ can be identified with the ionic hopping rate of the nuclear probe. In fact, the hopping of $^{7}$Li has proven to be well accessible with SAE-NMR in the range 1 $s^{-1}$ to $10^{4}$ $s^{-1}$, corresponding to slow motion in the low-temperature regime [42, 43].

Static $^{7}$Li NMR spectra of most materials suffer from strong dipolar broadening due to the high dipolar moment of the $^{7}$Li nucleus. Yet, the effect of Li motion can be studied qualitatively. The full width at half maximum value of the dominant central resonance ($m = 1/2 \leftrightarrow m = -1/2$ transition) shows a characteristic temperature dependence according to which it decreases from the so-called

rigid-lattice width of typically a few kHz to only a fraction of that width in the temperature regime of extreme narrowing over a range of several hundred K. The actual residual line width is determined by the inhomogeneity of the external magnetic field. The temperature dependence of the motionally induced averaging of the dipolar interaction between the nuclei can be fitted with a suitable model yielding an estimation of the activation energy of the hopping rate of the interacting nuclei [44].

For the slow Li conductors studied here the combination of the presented NMR techniques can typically be applied in a temperature range from room temperature to several hundred Kelvin giving access to diffusion parameters over several orders of magnitude.

# 3 Case studies – results and discussion

## 3.1 Lithium niobate

Lithium niobate ($LiNbO_3$) single crystals are one of the most technologically important synthetic oxides in science and technology due to their ferroelectric, photorefractive, piezoelectric, acousto-optical, and non-linear optical properties [45–47]. The investigation of Li self-diffusion and defect structure especially at low temperatures is important for various applications [48].

Crystalline $LiNbO_3$ exhibits a wide solid solution region between 44 mol% and 50.5 mol% $Li_2O$ [49]. Single crystals commonly produced by the Czochralski method [50] show the congruent composition of about 48.6 mol% $Li_2O$. However, using the vapor transport equilibration method the synthesis of near stoichiometric crystals is also possible [51]. Composition changes of $Li_2O$ within the solid solution range from the lithium-poor to the near stoichiometric composition result in significant changes of physical properties [52, 53]. These changes are expected to be in large parts the result of defect clusters, which are also responsible for the non-stoichiometry. For the realization of the congruent composition, the most reliable model consists of a niobium antisite atom which is compensated by four lithium vacancies, which can be written in Kröger–Vink notation as [54–56]

$$Nb_{Li}^{\cdots\cdot} + 4\, V_{Li}'.$$

Up to now, diffusion experiments on $LiNbO_3$ were done mainly by nuclear magnetic resonance (NMR) studies and also by impedance spectroscopy [2, 13, 57–63], while most of the data are limited to the high-temperature range above 880 K. There, diffusion is very fast and the defect complexes are destabilized.

The results on Li diffusion presented in this section were already published as indicated and are reviewed here. We investigated Li self-diffusion in congruent single crystals (48.6 % $Li_2O$) close to room temperature between 379 and 523 K by NR [27, 28], between 423 and 773 K by SIMS [34] and between 473 and 1073 K by impedance spectroscopy [37] (conversion of conductivity by the Nernst Einstein equation). SAE-NMR measurements were not possible due to the very low ionic mobility. The results are in excellent agreement with each other (see Figure 3). This demonstrates that Li alone may account for the overall electric conductivity in that range. The diffusivities can be described by the Arrhenius law with an activation enthalpy of 1.33 eV, which is interpreted as the migration energy of a single Li vacancy [34]. A deviation from the Arrhenius behavior at the lower end of the temperature scale, e.g. due to defect cluster formation was not observed. The activation energy is lower than that found in the high temperature range by SIMS experiments by about 30 % [64]. This can be explained by the fact that above 773 K significant vacancy formation according to the reaction

$$<LiNbO_3> \leftrightarrow 3Li_2O + 4V'_{Li} + Nb^{\cdot\cdot\cdot\cdot}_{Li},$$

may take place. The activation energy is then given by the sum of the migration enthalpy and the formation enthalpy. The diffusivities of (110) and (001) oriented

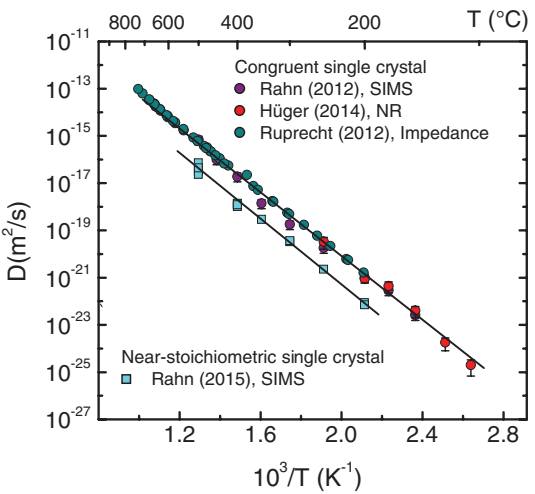


**Fig. 3:** Arrhenius plot of Li diffusivities in congruent $LiNbO_3$ single crystals (48.6 % $Li_2O$) and near-stoichiometric (49.9 % $Li_2O$) single crystals. The data correspond to Rahn et al. (2012) [34], Hüger et al. (2014) [27], Ruprecht et al. (2012) [37] measured on the same type of samples, and Rahn et al. (2015) [48].

single crystals are identical, proving the existence of a three-dimensional diffusion mechanism [65].

Results of SIMS measurements on near-stoichiometric (49.9 % $Li_2O$) $LiNbO_3$ single crystals (see also Figure 3) show diffusivities which are about one order of magnitude lower compared to the congruent $LiNbO_3$, while the activation energy is identical within error limits. This result is in agreement with the assumption of a $(Nb_{Li}^{\cdots\cdots} + 4V_{Li}')$ defect structure in order to explain off-stoichiometry [64]. The higher diffusivities of the congruent sample compared to the near-stoichiometric samples is simply due to a higher Li vacancy concentration. Details and more data can be found in [48].

In order to study the influence of structural disorder, SIMS experiments on amorphous lithium niobate films produced by ion-beam sputtering, were carried out between 293 and 423 K (see Figure 4) [66, 67]. Compared are samples which show a ratio of Li:Nb < 1 (Li-poor) and of Li:Nb >1 (Li-rich) in analogy to the stoichiometric composition of Li:Nb = 1 for crystalline $LiNbO_3$. The diffusivities of amorphous lithium niobate obey also the Arrhenius law with an activation enthalpy of 0.70 eV and 0.84 eV [66], respectively. The results show that the diffusivities of both types of amorphous samples are significantly (up to 10 orders of magnitude) higher than the diffusivities of the single crystal. This tremendous difference is traced back to the considerably lower activation energy of the amorphous samples. This is due to a lower packing density of the ions in the amorphous state

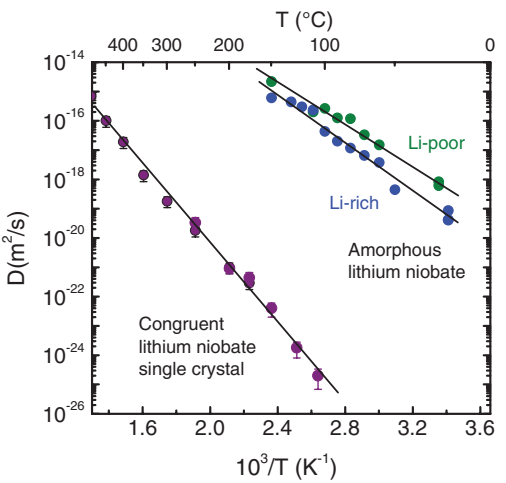


**Fig. 4:** Lithium diffusivities in amorphous lithium niobate (data partly from [66, 67]) as a function of reciprocal temperature in comparison to the diffusivities of a congruent lithium niobate single crystal (SIMS and NR data from Figure 3). For further details, see text.

and a lower mass density. The diffusivities of the amorphous samples containing a higher amount of Li are lower by a factor of about two to five. This demonstrates that a variation of the Li content in amorphous samples over the stability range of the crystalline $LiNbO_3$ phase has only a modest influence on diffusivities and activation enthalpies.

It is noted that a detailed comparison of the Li ion conductivities in the different structural forms of $LiNbO_3$ as model system, comprising nanocrystalline, amorphous as well as micro- and single-crystalline $LiNbO_3$, showed an overall behavior very similar to Figure 4 ([7], cf. Figure 5 therein).

## 3.2 Lithium orthoniobate

In order to investigate Li diffusion in a Li-rich compound in the system Li–Nb–O and to compare the results to those of $LiNbO_3$ we investigated the hitherto Li ion dynamics in $Li_3NbO_4$. The results are reported here. Two single crystals were grown via the Czochralski method at Institut für Kristallzüchtung, Berlin, Germany. One crystal was used for impedance spectroscopy measurements, the second crystal was cut into two pieces and used for NMR (crushed) and SIMS experiments, respectively. The part of the crystal used for SIMS was further cut into several small pieces and each investigated at different temperatures and/or annealing times.

The results are shown in Figure 5. As obvious, the different NMR methods are in good agreement to each other (activation energy 0.96 eV) but give significantly

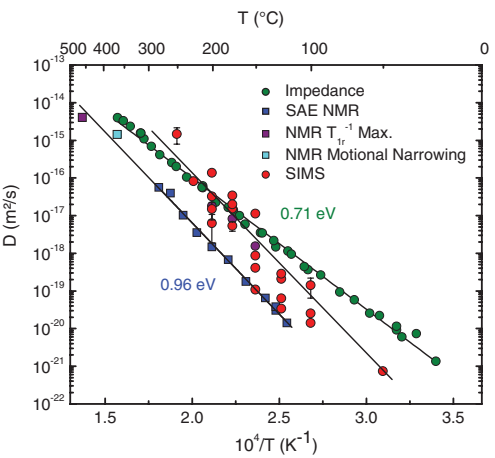


**Fig. 5:** Lithium diffusivities in $Li_3NbO_4$ as a function of reciprocal temperature as obtained by impedance spectroscopy NMR and SIMS. For further details, see text.

lower values than diffusivities derived from impedance spectroscopy (activation energy 0.71 eV), while the activation energy of the latter is lower. The results from SIMS (each data point from a different measurement) show a considerable scatter, but are mainly located in-between the data obtained by NMR and impedance measurements. Using SIMS data for a least-squares fit, an activation energy of 0.96 eV is obtained in agreement with the NMR data. This result can be explained by the fact that each part of the crystal has a different diffusivity varying up to two orders of magnitude. This assumption is supported by XRD measurements which show a strongly differing crystal orientation between the different parts investigated and also by EDX measurements which indicate different impurities (e.g. Mn content between 0.02 and 0.18 wt.%), however, in a non-systematic way. This means no homogeneous and pure single crystal was analyzed but more likely some type of polycrystal with an inhomogeneous distribution of impurities over the grown sample influencing diffusion. Consequently, the diffusivities in $Li_3NbO_4$ cannot be given exactly, only a range is obtained. The diffusivities are in average six orders of magnitude higher than in $LiNbO_3$, making the material interesting as an ion conductor. The activation energy is considerably lower.

## 3.3 Lithium tantalate

Lithium tantalate ($LiTaO_3$) has the same crystal structure as $LiNbO_3$ and is also used for applications in the field of optics and photonics [52]. Figure 6 shows new unpublished results of Li tracer diffusion measurements on (001) oriented

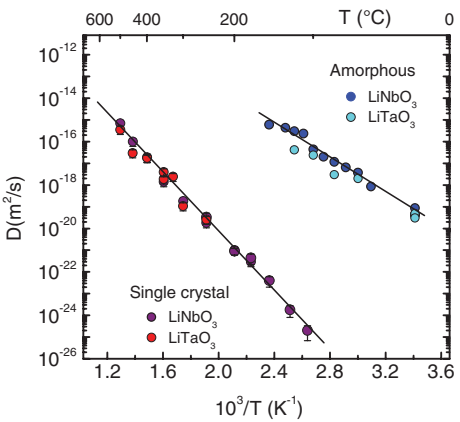


**Fig. 6:** Lithium diffusivities in $LiTaO_3$ and $LiNbO_3$ single crystals in comparison to amorphous counterparts as a function of reciprocal temperature.

single crystals and amorphous sputter layers in comparison to lithium niobate, as discussed above. The aim was to compare diffusion in materials with the same crystal structure but with different melting points and lattice parameters. In addition, it should be elucidated whether the substitution of Ta for Nb changes diffusion properties. As obvious, the diffusivities are very close to each other, possibly slightly lower than the corresponding results on lithium niobate. On first sight this is astonishing, because the two types of materials have different mass densities, melting points and lattice parameters. However, the Li ion density of $1.9 \times 10^{22}$ $cm^{-3}$ is also identical. This means Li–Li ion distances are similar. Further, the ionic radii of Nb and Ta are identical [68]. Consequently, the activation energies necessary for a Li jump are expected to be also similar and diffusion is taking place by nearly the same diffusivities. The same is true for the amorphous modification, emphasizing the fact that Li is migrating in a relatively robust and immobile skeleton of Nb(Ta)–O. For comparison with earlier results on the conductivities of micro- and nanocrystalline $LiTaO_3$ see Ref. [69].

## 3.4 Lithium aluminate

Lithium aluminate ($LiAlO_2$) is an important metal oxide for applications as a substrate and matching material for the epitaxial growth of semiconductors in light emitting diodes [70, 71], in nuclear technology as blanket material [72, 73] and finally as an additive in polymer electrolytes [74], as inert electrolyte support material in molten carbonate fuel cells [74], and as coating material for electrodes in Li-ion batteries [75]. For all of these applications, the diffusivity of Li close to room temperature is an important factor for the design, stability and performance of $LiAlO_2$ based devices.

Crystalline lithium aluminate occurs in several different structural modifications, which are mainly established as high pressure phases [76]. At ambient pressure the tetragonal $\gamma$-$LiAlO_2$ phase (P422, $a = 5.169$ Å, $c = 6.268$ Å, $\rho = 2.61$ g/cm$^3$) [77] is stable. This phase can also be produced commercially as a single crystal. Since the 1980's fundamental investigations on $\gamma$-$LiAlO_2$ polycrystals were done by dc conductivity measurements and NMR which are summarized in [78]. In different studies, a low activation enthalpy of 0.7–0.8 eV at temperatures below 1036 and a higher activation enthalpy of 1.0–1.3 eV at temperatures above 1063 K were found [79, 80]. While the first one was attributed to extrinsic diffusion, the second one was interpreted with intrinsic diffusion behavior. More recent dc conductivity studies [81] found the higher activation enthalpy also at lower temperatures and in single crystals, while NMR on the same types of samples give a broad spectrum

of activation enthalpies between 0.7 and 1.12 eV for different NMR methods [81]. This indicates that different Li jumps are probed. A quite recent study on microcrystalline γ-$LiAlO_2$ [82] with nearly the whole arsenal of NMR methods including SAE and SLR in the rotating reference frame, which are sensitive at low temperatures, as well as impedance spectroscopy consistently, yielded an activation energy of 0.7 eV.

The results on Li diffusion presented in this section were again already published as indicated and are reviewed here. We carried out an investigation of Li diffusion in γ-$LiAlO_2$ single crystals by combining SIMS and impedance spectroscopy as well as neutron powder diffraction and theoretical calculations [78]. In this study, an activation energy of 1.1–1.2 eV between 373 and 673 K was found from the first two methods in excellent agreement (see Figure 7). From neutron diffraction data, both on the powder and independently on a single crystal [84], a strongly curved diffusion path between adjacent Li positions was deduced. A migration barrier of 0.72 eV was identified and attributed to a vacancy mechanism [78]. The resulting very low vacancy formation energy of only 0.48 eV is traced back to the fact that mobile defects are not generated from ideal domains but from preformed structural defects (twin boundaries, small amounts of dopants) [78].

In addition, there are recent measurements on lithium self-diffusion in amorphous lithium aluminate layers as prepared by ion-beam sputtering (Figure 7). The samples were characterized between room temperature and 473 K [83]. Diffusion profiles were analysed by SIMS. The results show that the diffusivities obey the Arrhenius law with an activation energy of 0.94 eV. This value is not much

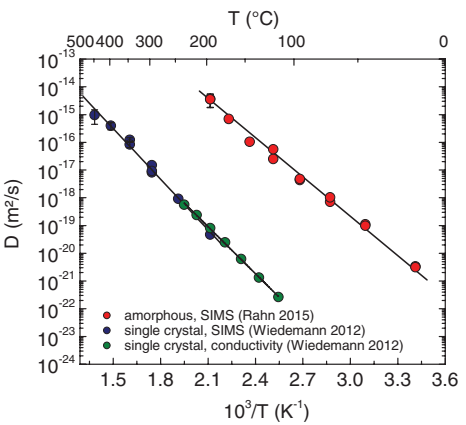


**Fig. 7:** Lithium diffusivities in γ-$LiAlO_2$ single crystals (Wiedemann et al. [78]) in comparison to amorphous lithium aluminate as a function of reciprocal temperature (Rahn et al. [83]).

different from the activation energy of 1.20 eV found for $LiAlO_2$ single crystals by SIMS and explains the only modest enhancement of diffusivities in amorphous lithium aluminate by three to five orders of magnitude in the temperature range studied, when compared e.g. to the lithium niobate system.

## 3.5 Lithium gallate

Finally, we carried out investigations of Li diffusion in β-$LiGaO_2$ single crystals. This compound has attracted interest due to the fact that it is a lattice-matching substrate currently being considered for GaN heteroepitaxy, which offers distinct advantages toward growth of high quality GaN [85]. It is also a promising lattice-matching substrate for heteroepitaxy of ZnO [86] and InN [87].

In contrast to γ-$LiAlO_2$, single crystals are available in an orthorombic wurzite-like structure ($Pna2_1$, a = 5.402 Å, b = 6.372 Å, c = 5.007 Å, ρ = 4.19 g/cm³) [88, 89]. The (001) oriented crystal was obtained from the Leibniz-Institut für Kristallzüchtung, Berlin (Germany). In Figure 8 diffusivities of single crystals (between 573 and 773 K) and of ion-beam sputtered amorphous films (between 293 and 573 K) are compared. These results, presented for the first time here, were obtained by the SIMS method. Literature data on Li diffusivities in this type of material were not known beforehand. The situation is similar to the case of $LiAlO_2$. While the diffusivities of the amorphous modification are enhanced by

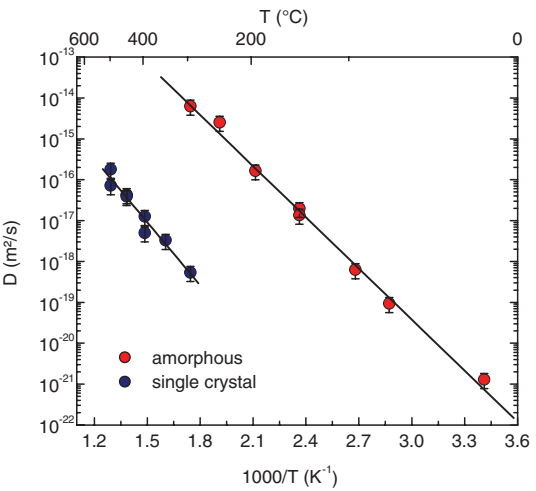


**Fig. 8:** Lithium diffusivities in β-$LiGaO_2$ single crystals in comparison to amorphous lithium gallate as a function of reciprocal temperature.

about four orders of magnitude compared to the single crystal, the activation enthalpies are quite similar. Values of (1.04 ± 0.1) eV are found for the single crystal and (0.83 ± 0.04) eV for the amorphous film, respectively, leading to an only modest enhancement of diffusivities in the latter structure. The absolute values of the diffusivities are lower by one order of magnitude in the lithium gallate system than in the lithium aluminate system for single crystals and amorphous films.

NMR experiments have been carried out on polycrystalline β-$LiGaO_2$ samples prepared from solid-state synthesis (ss-) and from powdered single crystals of β-$LiGaO_2$ (cr-) [90]. While the ss-$LiGaO_2$ sample had an average particle size of 5μm, cr-$LiGaO_2$ consisted of particles of 100 μm of average size. The surface defect concentration is expected to be higher for ss-$LiGaO_2$. These differences are also reflected in the $^7$Li NMR spin-lattice relaxation behavior but both samples show NMR signatures corresponding to single crystallographic sites for Li and Ga. The ss-$LiGaO_2$ sample was used to study the motional narrowing behavior of the $^7$Li central transition signal. A motional narrowing representing all Li ions in the system did not occur in the measurement temperature range (293–473 K). However, a small portion of Li ions in the system participated in a localized dynamic process. This was reflected as a partial averaging of the Li–Li dipolar interaction, representing only a small fraction of the total Li ions involved in a to-and-fro jump process [90].

Further, an analysis using $^7$Li SAE experiments to probe slow dynamic modes in the system was done. The ss-$LiGaO_2$ system showed Arrhenius type behavior of slow Li ionic jump rates between 373 and 448 K. The slope of the linear fit yielded a very low activation energy of 0.13 eV only, in contrast to the SIMS measurements at higher temperatures. This indicates the presence of a localized dynamic process or a to-and-fro jump process of the probed species. For comparison, the SAE experiments were also done on the cr-$LiGaO_2$ system in the same temperature range. The ionic jump rates obtained here were in the same order as in the case of ss-$LiGaO_2$ ($10^0 \ldots 10^1$ $s^{-1}$), but the activation energy was higher (0.40 eV). However, γ-$LiAlO_2$ and β-$LiGaO_2$ are considered to have similar dynamic properties despite of their differences in structure. An activation energy of 0.40 eV in the case of $LiGaO_2$ is smaller than that observed for $LiAlO_2$ (0.70 eV). Therefore, this could also be an indication of a localized jump process in cr-$LiGaO_2$ [90].

In short, the overall ion diffusion processes in the $LiGaO_2$ system, observable with NMR methods, can only be activated at temperatures above 473 K. However, measurements at temperatures below allow one to monitor localized (to-and-fro) ion jump processes involving a small fraction of the total Li ions only.

# 4 Conclusion

In conclusion, experimental investigation of Li self-diffusion in various lithium containing metal oxides ($LiNbO_3$, $Li_3NbO_4$, $LiTaO_3$, $LiAlO_2$, and $LiGaO_2$) were carried out by secondary ion mass spectrometry and neutron reflectometry as well as nuclear magnetic resonance spectroscopy and impedance spectroscopy. The results revealed that a combination of macroscopic tracer methods and microscopic methods give a comprehensive insight into slow diffusion processes, especially for materials with different structural disorder.

**Acknowledgements:** Financial support from the Deutsche Forschungsgemeinschaft (DFG) in the framework of the Research Unit FOR 1277 ("molife") (Schm 1569/18 and He 1574/13) is gratefully acknowledged. The authors thank R. Uecker for providing the $LiGaO_2$ and $Li_3NbO_4$ single crystals as well as W. Gruber and B. Jerliu for their assistance in XRD analysis and sputter deposition.

# References

1. H. Schmidt, M. Gupta, T. Gutberlet, J. Stahn, M. Bruns, Acta Mater. **56** (2008) 464.
2. M. Wilkening, P. Heitjans, Solid State Ionics **177** (2006) 3031.
3. R. Böhmer, J. Magn. Reson. **147** (2000) 78.
4. F. Qi, C. Rier, R. Böhmer, W. Franke, P. Heitjans, Phys. Rev. B **72** (2005) 104301.
5. R. Böhmer, T. Jörg, F. Qi, A. Titze, Chem. Phys. Lett. **316** (2000) 419.
6. M. Wilkening, P. Heitjans, Phys. Rev. B **77** (2008) 24311.
7. M. Wilkening, P. Heitjans, Chem. Phys. Chem. **13** (2012) 53.
8. K. Funke, C. Cramer, D. Wilmer, In: Diffusion in Condensed Matter – Methods, Materials, Models (Eds. P. Heitjans and J. Kärger), Springer, Berlin (2005), P. 857.
9. M. Månsson, J. Sugiyama, Phys. Scr. **88** (2013) 68509, and references therein.
10. C. V. Chandran, P. Heitjans, Annu. Rep. NMR Spectrosc. **89** (2016) 1.
11. W. A. MacFarlane, Solid State Nuc. Magn. Reson. **68–69** (2015) 1.
12. P. Heitjans, A. Schirmer, S. Indris, In: Diffusion in Condensed Matter – Methods, Materials, Models (Eds. P. Heitjans and J. Kärger), Springer, Berlin (2005), P. 367.
13. P. Heitjans, M. Masoud, A. Feldhoff, M. Wilkening, Faraday Discuss. **134** (2007) 67.
14. Y. Saito, H. Yamamoto, O. Nakamura, H. Kageyama, H. Ishikawa, T. Miyoshi, M. Matsuoka, J. Power Sources **81–82** (1999) 772.
15. R. Böhmer, K. R. Jeffrey, M. Vogel, Prog. Nucl. Magn. Reson. Spectrosc. **50** (2007) 87.
16. M. Masoud, P. Heitjans, Defect Diffus. Forum **237–240** (2005) 1016.
17. S.-C. Jeong, I. Katayama, H. Kawakami, Y. Watanabe, H. Ishiyama, N. Imai, Y. Hirayama, H. Miyatake, M. Sataka, H. Sugai, S. Okayasu, S.-I. Ichikawa, K. Nishio, S. Mitsuoka, T. Nakanoya, T. Hashimoto, M. Yahagi, T. Hashimoto, Jpn. J. Appl. Phys. **47** (2008) 6413.
18. T. Okumura, T. Fukutsuka, Y. Uchimoto, N. Sakai, K. Yamaji, H. Yokokawa, J. Power Sources **189** (2009) 643.

19. Y. Oishi, Y. Kamei, M. Akiyama, T. Yanagi, J. Nuc. Mater. **87** (1979) 341.
20. Du Yongjuan, G. H. Frischat, W. Beier, J. Non-Cryst. Solids **112** (1989) 399.
21. A. Buksak, G. H. Frischat, G. Heide, J. Non-Cryst. Solids **353** (2007) 2447.
22. M. Gupta, Phys. Rev. B **70** (2004) 184206.
23. J. Speakman, P. Rose, J. A. Hunt, N. Cowlam, R. E. Somekh, A. L. Greer, J. Magn. Magn. Mater. **156** (1996) 411.
24. S. Chakravarty, M. Jiang, U. Tietze, D. Lott, T. Geue, J. Stahn, H. Schmidt, Acta Mater. **59** (2011) 5568.
25. E. Hüger, U. Tietze, D. Lott, H. Bracht, D. Bougeard, E. E. Haller, H. Schmidt, Appl. Phys. Lett. **93** (2008) 162104.
26. H. Schmidt, Phys. Rev. Lett. **96** (2006) 55901.
27. E. Hüger, J. Rahn, J. Stahn, T. Geue, P. Heitjans, H. Schmidt, Phys. Chem. Chem. Phys. **16** (2014) 3670.
28. E. Hüger, J. Rahn, J. Stahn, T. Geue, H. Schmidt, Phys. Rev. B **85** (2012) 214102.
29. H. Mehrer, Diffusion in Solids: Fundamentals, Methods, Materials, Diffusion-Controlled Processes, Springer, Berlin (2007).
30. H. Schmidt, Phys. Rev. B **74** (2006) 45203.
31. H. Schmidt, G. Borchardt, C. Schmalzried, R. Telle, S. Weber, H. Scherrer, J. Appl. Phys. **93** (2003) 907.
32. R. Kube, H. Bracht, E. Hüger, H. Schmidt, Phys. Rev. B **88** (2013) 85206.
33. H. Bracht, E. Haller, R. Clark-Phelps, Phys. Rev. Lett. **81** (1998) 393.
34. J. Rahn, E. Hüger, L. Dörrer, B. Ruprecht, P. Heitjans, H. Schmidt, Phys. Chem. Chem. Phys. **14** (2012) 2427.
35. J. Crank, The Mathematics of Diffusion, Oxford University Press, Oxford (1979).
36. C. Braun, Parratt32 – The reflectivity tool: The manual, version 1.6.0, HMI Berlin (1997–2002).
37. B. Ruprecht, J. Rahn, H. Schmidt, P. Heitjans, Z. Phys. Chem. **226** (2012) 431.
38. B. Ruprecht, Langsamer Li-Transport in Lithiumübergangsmetalloxiden untersucht mit NMR- und impedanzspektroskopischen Methoden: Dissertation, Leibniz Universität Hannover, 2012, http://d-nb.info/1028873123/04.
39. N. Bloembergen, E. M. Purcell, R. V. Pound, Phys. Rev. **73** (1948) 679.
40. M. B. Salamon, Physics of Superionic Conductors, Springer, Berlin (1979).
41. J. Jeener, P. Broekaert, Phys. Rev. **157** (1967) 232.
42. B. Ruprecht, M. Wilkening, R. Uecker, P. Heitjans, Phys. Chem. Chem. Phys. **14** (2012) 11974.
43. M. Wilkening, R. Amade, W. Iwaniak, P. Heitjans, Phys. Chem. Chem. Phys. **9** (2007) 1239.
44. J. Hendrickson, P. Bray, J. Magn. Reson. **9** (1973) 341.
45. T. Volk, M. Wöhlecke, Lithium Niobate: Defects, Photorefraction and Ferroelectric Switching, Springer, Berlin (2008).
46. M. C. Gupta, J. Ballato (Eds.), The Handbook of Photonics, 2nd ed., CRC Press, Boca Raton (2007).
47. K. K. Wong (Ed.), Properties of Lithium Niobate, INSPEC/Institution of Electrical Engineers, London (2002).
48. J. Rahn, P. Heitjans, H. Schmidt, J. Phys. Chem. C **119** (2015) 15557.
49. P. Lerner, C. Legras, J. P. Dumas, J. Cryst. Growth **3–4** (1968) 231.
50. H. H. Kusuma, D. P. N. Made, M. R. Sudin, M. S. Rohani, AIP Conf. Proc. **1217** (2010) 182.
51. P. F. Bordui, R. G. Norwood, D. H. Jundt, M. M. Fejer, J. Appl. Phys. **71** (1992) 875.
52. V. Gopalan, M. C. Gupta, J. Appl. Phys. **80** (1996) 6099.
53. V. Gopalan, T. E. Mitchell, Y. Furukawa, K. Kitamura, Appl. Phys. Lett. **72** (1998) 1981.

54. J. Shi, H. Fritze, G. Borchardt, K.-D. Becker, Phys. Chem. Chem. Phys. **13** (2011) 6925.
55. R. M. Araujo, K. Lengyel, R. A. Jackson, L. Kovács, M. E. G. Valerio, J. Phys.: Condens. Matter **19** (2007) 46211.
56. H. Xu, D. Lee, S. B. Sinnott, V. Dierolf, V. Gopalan, S. R. Phillpot, J. Phys.: Condens. Matter. **22** (2010) 135002.
57. D. Bork, P. Heitjans, J. Phys. Chem. B **102** (1998) 7303.
58. M. Wilkening, D. Bork, S. Indris, P. Heitjans, Phys. Chem. Chem. Phys. **4** (2002) 3246.
59. T. K. Halstead, J. Chem. Phys. **53** (1970) 3427.
60. A. Mehta, E. K. Chang, D. M. Smyth, J. Mater. Res. **6** (1991) 851.
61. D. Bork, P. Heitjans, J. Phys. Chem. B **105** (2001) 9162.
62. G. Bergmann, Solid State Commun. **6** (1968) 77.
63. A. V. Yatsenko, S. V. Yevdokimov, A. S. Pritulenko, D. Y. Sugak, I. M. Solskii, Phys. Solid State **54** (2012) 2231.
64. D. P. Birnie, J. Mater. Science **28** (1993) 302.
65. J. Rahn, L. Dörrer, B. Ruprecht, P. Heitjans, H. Schmidt, Defect Diffus. Forum **333** (2013) 33.
66. J. Rahn, B. Ruprecht, P. Heitjans, H. Schmidt, Defect Diffus. Forum **363** (2015) 62.
67. J. Rahn, E. Hüger, L. Dörrer, B. Ruprecht, P. Heitjans, H. Schmidt, Z. Phys. Chem. **226** (2012) 439.
68. I. Inbar, R. E. Cohen, Phys. Rev. B **53** (1996) 1193.
69. M. Wilkening, V. Epp, A. Feldhoff, P. Heitjans, J. Phys. Chem. C **112** (2008) 9291.
70. J. W. Gerlach, A. Hofmann, T. Höche, F. Frost, B. Rauschenbach, G. Benndorf, Appl. Phys. Lett. **88** (2006) 11902.
71. L. Wang, E. Richter, M. Weyers, Phys. Stat. Sol. (a) **204** (2007) 846.
72. J.-P. Jacobs, M. A. San Miguel, L. J. Alvarez, P. B. Giral, J. Nucl. Mater. **232** (1996) 131.
73. J. Lin, Z. Wen, X. Xu, N. Li, S. Song, Fusion Eng. Des. **85** (2010) 1162.
74. S. Terada, I. Nagashima, K. Higaki, Y. Ito, J. Power Sources **75** (1998) 223.
75. H. Cao, B. Xia, Y. Zhang, N. Xu, Solid State Ionics **176** (2005) 911.
76. L. Lei, D. He, Y. Zou, W. Zhang, Z. Wang, M. Jiang, M. Du, J. Solid State Chem. **181** (2008) 1810.
77. M. Marezio, Acta Crystallogr. **19** (1965) 396.
78. D. Wiedemann, S. Nakhal, J. Rahn, E. Witt, M. M. Islam, S. Zander, P. Heitjans, H. Schmidt, T. Bredow, M. Wilkening, M. Lerch, Chem. Mater. **28** (2016) 915.
79. T. Matsuo, H. Ohno, K. Noda, S. K. Oonishi, H. Yoshida, H. Watanabe, J. Chem. Soc., Faraday Trans. 2 **79** (1983) 1205–1216.
80. S. Konishi, H. Ohno, J. Amer. Ceram. Soc. **67** (1984) 418.
81. S. Indris, P. Heitjans, R. Uecker, B. Roling, J. Phys. Chem. C **116** (2012) 14243.
82. E. Witt, S. Nakhal, C. V. Chandran, M. Lerch, P. Heitjans, Z. Phys. Chem. **229** (2015) 1327.
83. J. Rahn, E. Witt, P. Heitjans, H. Schmidt, Z. Phys. Chem. **229** (2015) 1341.
84. D. Wiedemann, S. Indris, M. Meven, B. Pedersen, H. Boysen, R. Uecker, P. Heitjans, M. Lerch, Z. Krist. – Cryst. Mater. **231** (2016) 189.
85. S. W. Seo, K. K. Lee, S. Kang, S. Huang, W. A. Doolittle, N. M. Jokerst, A. S. Brown, Appl. Phys. Lett. **79** (2001) 1372.
86. T. Huang, S. Zhou, H. Teng, H. Lin, J. Wang, P. Han, R. Zhang, J. Crys. Growth **310** (2008) 3144.
87. G. Li, H. Yang, Cryst. Growth Des. **11** (2011) 664.
88. C. Chen, C.-A. Li, S.-H. Yu, M. M. Chou, J. Cryst. Growth **402** (2014) 325.
89. M. Marezio, Acta Cryst. **18** (1965) 481.
90. C. Vinod Chandran, K. Volgmann, S. Nakhal, R. Uecker, E. Witt, M. Lerch, P. Heitjans, Z. Phys. Chem. **231** (2017) 1423.